IBRACON Structures and Materials Journal
Revista IBRACON de Estruturas e Materiais
ISSN 1983-4195 ismj.org

ORIGINAL ARTICLE

Damage assessment & innovation of efficient retrofitting solution of RC slabs exposed to contact explosion

Avaliação de danos e inovação de solução eficiente de reabilitação de lajes de concreto armado expostas a explosão de contato

Ibrahim Mohamed Metwally[a]

[a]Housing & Building National Research Center, Concrete Structures Research Institute, Dokki, Giza, Egypt

Received 03 February 2022
Accepted 15 August 2022

Abstract: Under contact explosions, the reinforced concrete structures can behave in a brittle manner with highly localized damage like concrete cratering, spalling, and reinforcement rupturing. High-speed fragmentation resulting from concrete spall may cause severe casualties and injuries. It is therefore important to restrained concrete fragments and improve collapse resistance of the slab. A new retrofitting technique is proposed in this paper which completely prevents fragmentation. To mitigate blast effects on civil structures, a new kind of concrete material named Ultra-High-Performance-Concrete (UHPC) is now widely studied and applied. UHPC material is known for its high compressive and tensile strength, large energy absorption capacity as well as good workability and anti-abrasion ability compared to normal strength concrete(NRC). All of recent experimental published work concerning blast performance of UHPC slabs under far or near explosion effect, on the other side, the contact explosion tests are relatively limited experimentally and nearly impossible because of security restrictions and costly in terms of both preparation and measurements. So, the real and accurate finite element models are needed to address this gap and understanding the real contact-explosion behavior of both NRC and UHPC slabs. The numerical analyses allow gaining insight into the complex failure mechanisms occurring in the slab and not directly observable. In this study, coupled smoothed particle hydrodynamics (SPH) method and finite element method is utilized to simulate the contact blast tests. Numerical results are compared with the experimental observations, and the feasibility and accuracy of the numerical model are validated. The validated numerical model provided a useful tool for designing potential blast-retrofitting solutions which can prevent the local material damage and fragmentations in both NRC & UHPC slabs subjected to contact explosion. This study introduced adequate and very efficient protection solution for both NRC & UHPC slabs exposed to contact explosion (1 kg of TNT) by utilizing the composite action generated between slabs & bonded steel plates. The 2 mm and 1 mm bonded steel plates at both faces of the NRC and UHPC slabs respectively attained a superior resistance to contact explosion.

Keywords: UHPC, contact explosion, slabs, Ansys Workbench.

Resumo: Sob explosões de contato, as estruturas de concreto armado podem se comportar de forma frágil com danos altamente localizados, como crateras de concreto, “spalling” e ruptura de reforço. A fragmentação em alta velocidade resultante de “spalling” de concreto pode causar graves mortalidades e ferimentos. Por isso, é importante conter fragmentos de concreto e melhorar a resistência ao colapso da laje. Uma nova técnica de reabilitação é proposta neste artigo que impede completamente a fragmentação. Para mitigar os efeitos da explosão nas estruturas civis, um novo tipo de material concreto chamado Ultra-High-Performance-Concrete (UHPC) é agora amplamente estudado e aplicado. O material UHPC é conhecido por sua alta resistência à compressão e tração, grande capacidade de absorção de energia, bem como boa trabalhabilidade e resistência à abrasão em comparação com o concreto de resistência normal (NRC). Todos os trabalhos publicados experimentais recentes sobre o desempenho das lajes UHPC consideram o efeito de uma explosão longe ou muito perto, por outro lado, os testes de explosão de contato são relativamente limitados experimentalmente e quase impossíveis devido a restrições de segurança e dispendiosos em termos de preparação e medições. Assim, os modelos reais e precisos de elementos finitos são necessários para resolver essa lacuna e entender o comportamento real de explosão de contato das lajes NRC e UHPC. As análises numéricas permitem obter informações sobre os complexos mecanismos de falha que ocorrem na laje e não diretamente observáveis.

Corresponding author: Ibrahim Mohamed Metwally. E-mail: ibrahimhbrc@gmail.com
Financial support: None.
Conflict of interest: Nothing to declare.
Data Availability: The data that support the findings of this study are openly available in reference list at the end of this paper.

Neste estudo, o método de hidrodinâmica de partículas suavizadas (SPH) e o método de elemento finito são utilizados para simular os testes de explosão de contato. Os resultados numéricos são comparados com as observações experimentais, e a viabilidade e a precisão do modelo numérico são validadas. O modelo numérico validado forneceu uma ferramenta útil para projetar soluções potenciais de adaptação de explosão que podem evitar danos e fragmentações de materiais locais em ambas as lajes NRC e UHPC submetidas à explosão de contato. Este estudo introduziu uma solução de proteção adequada e muito eficiente para ambas as lajes NRC e UHPC expostas à explosão de contato (1 kg de TNT) utilizando a interação composta gerada entre lajes e placas de aço ligados. As chapas de aço coladas de 2 mm e 1 mm em ambas as faces das lajes NRC e UHPC, respectivamente, obtiveram uma resistência superior à explosão de contato.

Palavras-chave: UHPC, explosão de contato, lajes, Ansys Workbench.

How to cite: I. M. Metwally, "Damage assessment & innovation of efficient retrofitting solution of RC slabs exposed to contact explosion," *Rev. IBRACON Estrut. Mater.*, vol. 16, no. 2, e16207, 2023, https://doi.org/10.1590/S1983-41952023000200007

1 INTRODUCTION

Under explosive loading conditions, various failure modes can be observed on reinforced concrete structures, including bending failure, shear failure and concrete spalling failure. Flexural damage is the most ideal damage mechanism because it has the greatest ductility and can absorb energy to the greatest extent. In addition to bending and shearing damage, concrete spalling is another important damage mode, which mainly occurs at close range or in contact with explosion [1], [2].

When subjected to explosive loadings, the concrete structures may present local damage, including cratering, spalling and breaching damage. As shown in Figure 1, cratering damage occurs because of high compressive pressure in the contacted surface between the concrete and charges. Spalling damage appears in the free surface of the concrete structures when the tensile stress generated by the compressive waves in the free surface is larger than the spalling strength of the concrete. Breaching damage arises when the impulse generated by the explosion is large enough to overcome the resistant forces of structures [1].

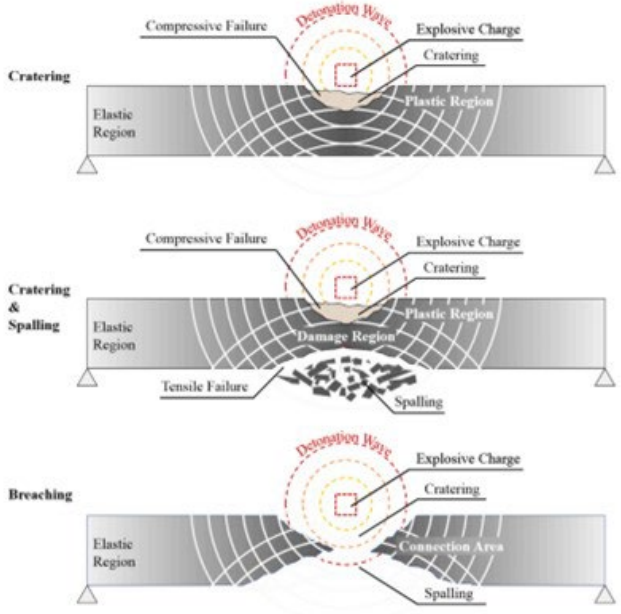

Figure 1- Cratering, spalling and breaching damage of concrete structures exposed to contact explosion [2].

In the blast event, the high-speed fragments produced by the spalling and breaching damage of structures could cause unexpected casualties and property loss [3]–[5]. Therefore, it is most significant to prevent and decrease the spalling and breaching damage of the structures under blast loadings. To solve this problem, Morishita et al. [6], as well as Tanaka and Tuji [7] attempted to increase the reinforcement ratio and compressive strength of concrete to obtain an outstanding blast resistance of concrete structures, but the results of the tests were not consistent with the desired effect.

In the protective structures against blast loadings, Nam et al. [8] found that the energy absorption capacity and the fracture energy of materials have an obvious influence on the blast resistance performance of structures. Ultra-high performance concrete (UHPC) has a compressive strength of 150–250 MPa and a flexural strength of 30–40 MPa. It has exceptionally high energy absorption capacity compared to NRC and has resistance to fragmentation, making it ideal for panels and components that need to perform under explosive, impact or shock loads. Besides, it also shows excellent fracture energy with 20,000–40,000 J/m^2, which is several orders of magnitude higher than that of normal concrete materials. Its flexural toughness is greater than 200 times that of conventional fiber reinforced concrete. That indicates UHPC can be employed to prevent and decrease spalling damage. Furthermore, UHPC presents better durability, fire performance, the excellent cyclic, fatigue and impact performance [9].

Because of previous advantages of UHPC, it could have great prospects in the engineering structures against blast loadings. It is regretted that only few researches were conducted on the spalling resistant performance of UHPC. The primary purpose of conducting the blast tests and numerical analysis of UHPC is to provide adequate structural protection against explosions.

The response of reinforced concrete (RC) members subjected to contact explosion effects is more severe than the response to non-contact explosions due to local material failure. The shock-wave reflection within the RC member causes severe local material damage. The resulting loss of concrete cross-section reduces the axial load and bending capacity of the RC member. Therefore, it is of great significance to study the local damage and fragments of RC members under contact explosions. The response of RC components to contact explosion effects is highly non-linear and is an ongoing field of study. Besides, mitigation of contact explosion effects is yet to be studied. Therefore, it is imperative to design strategically important structures envisaged as a potential target for terrorist attacks by incorporating mitigation strategies that limit the damage caused by contact explosions.

Based on the excellent energy absorption property and high fracture energy of UHPC, it is promising to prevent and decrease the spalling damage. Moreover, the test results conducted by Li et al. [10] can also provide data for calibrating and verifying the dynamic constitutive model of UHPC. In this study, two UHPC slabs and one NRC slab as a control one were prepared, by Li et al. [10]. 1 kg TNT explosives were employed to generate the contact-blast loadings. The primary objective of this research is to develop an accurate numerical model to simulate the real behavior, damage mechanism, & fragmentation of NRC & UHPC reinforced concrete slabs under contact explosion, and comparing the numerical results with those obtained by the tests of the slab specimens of the experiments conducted by Li et al. [10] for validation of the proposed model. Besides, promising retrofitting technique that have shown impressive results for fragmentations prevention.

2 DESCRİPTİON OF SLAB TESTS

For a more comprehensive description of the slab tests including slab specimens, materials properties, experimental procedure and test setup, instrumentation, as well as description of the test results including damage patterns, reinforcement strains & fragmentations can be found as detailed by the work of Li et al. [10]. In total, three slabs including one normal strength concrete (NRC-2) slab and two micro steel fiber reinforced ultra-high performance concrete (UHPC-4 & UHPC-7) slabs were tested [10]. The dimension of all slabs is: 2000 mm long, 800 mm wide and 120 mm thick. UHPC-4 slab was longitudinally reinforced by 9D12, while UHPC-7 slab was reinforced by less longitudinal reinforcement bars (5D12). This modification was made to investigate the influence of longitudinal reinforcement spacing on slab response. The shear reinforcement for all slab are constant equal 11D8. Both of these two reinforcements (D12 & D8) have 360 MPa yielding strength. Table 1 and Figure 2 show the slab concrete dimensions and reinforcement. The control NRC slabs were constructed by concrete with unconfined compressive strength of 40 MPa, while UHPC concrete made with micro steel fibers with a length of 15 mm and diameter of 0.12 mm were mixed at a volume dosage of 2.5%; the tensile strength of the micro steel fiber is 4295 MPa. Ultra-high performance fiber reinforced concrete with uniaxial compressive strength of 145 MPa and tensile strength of 22 MPa was used to build the UHPC slabs [10].

Table 1-Summary of slab specimens tested by Li et a [10]

Specimen	Slab thickness, mm	Compressive strength of concrete, MPa	Longitudinal reinforcement	Shear reinforcement	Observed damage mode
NRC-2	120	40	9D12	11D8	Perforation
HPC-4	120	145	9D12	11D8	Perforation
UHPC-7	120	145	5D12	11D8	Perforation

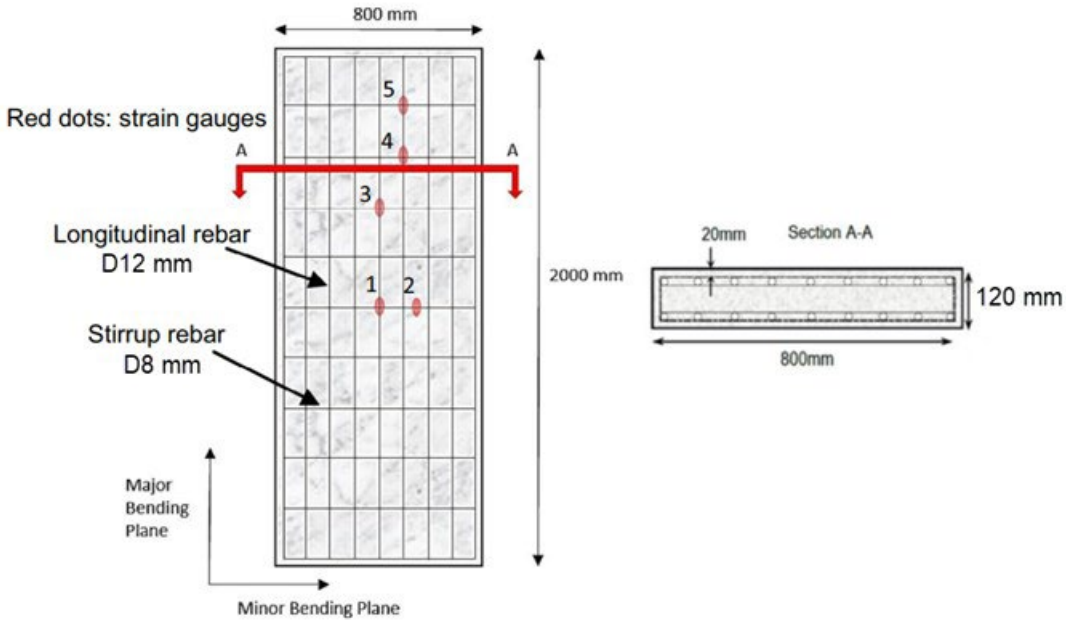

Figure 2 - Reinforcement layout of slab specimens tested by Li et al. [10]

3 EXPERIMENTAL SETUP

As depicted in Figure 3, the slab was firstly placed on the steel rig using a crane, then both ends of the slab were bolt fixed with the angle steel cleats. The slab was subjected to contact explosions of cylindrical explosives of and 1 kg of TNT. During the sample preparation, strain gauges were attached to the reinforcement bars at different locations of each slab as indicated by red dots in Figure 2. The positions where the strain gauges located were carefully grinded using electrical grinder, and later mopped using liquid acetone. These procedures were carried out to guarantee the contact between the strain gauge and reinforcing bar. Strain gauges were used to record the strain time history [10].

Figure 3 - Test setup of the slab specimens tested by Li et al. [10]

4 FİNİTE ELEMENT MODELİNG & ANALSİS

In this study, both NRC & UHPC slab specimens tested by Li et al. [10] under contact explosion are numerically modeled and analyzed using ANSYS Workbench Explicit Dynamic module [11]. A three-dimensional finite element model has been created for the slabs with the use of the Explicit Dynamics Lagrangian formulation. The detailed modeling steps are described in the following sections.

4.1 Geometry

The ANSYS Workbench Design Modeler, which provides analysis-specific geometry modeling tools, has been used to model the specimens. The concrete slabs with dimensions of 2000 × 800 × 120 mm and 1 kg TNT explosion material have been modeled using the hexahedron solid body. The shape of TNT charge in the experimental test was cylindrical shape (Figure 2), in the present study, a cubical shape was used in all FE models. This based on the findings of Zhao et al. [12] that is using the cubic charge instead of the cylinder charge is allowable and don't affect the damage mechanism and performance of RC slab exposed to contact explosion. The reinforcement bars have been modeled using discrete line body (Beam Elements) objects and were placed in exact coordinates matching their respective locations as of Figures 2 and 4. The created geometry model for the whole problem using ANSYS Design Modeler is illustrated in Figure 4. This model is then imported by the Explicit Dynamics system to continue with the modeling and analysis steps.

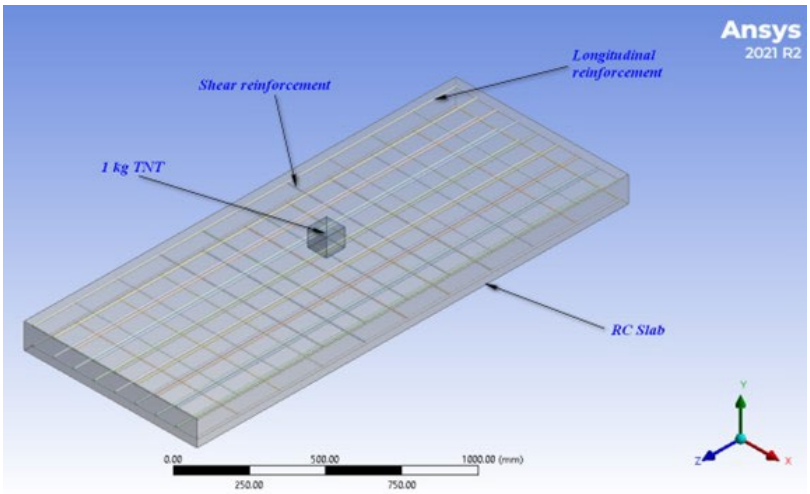

Figure 4- Geometry model of the reinforcement discrete line bodies(beam elements) embedded within the concrete slab solid body of the slab specimens under contact explosion tested by Li et al. [10]

4.2 Material Modeling

4.2.1 Constitutive model of concrete

ANSYS explicit materials library has two concrete materials named as CONC-35 and CONC-140 in addition to CONCRETE-L material model. These models have advanced plasticity options for brittle materials covered by the RHT concrete strength [13] which is expressed in terms of pressure dependent initial elastic yield surface, failure surface and residual friction surface in the stress space. The mathematical description of RHT model, descriptions of the parameters such as polynomial equation of state (EOS) parameters, damage parameters, and failure surface parameters and their default values corresponding to standard 35 MPa concrete can be found in Borrvall and Riede [14]. The RHT constitutive model is an advanced plasticity and shear damage model. Similar to other hydrodynamic codes, the study of the dynamic response of materials and structures involves the governing equations and in ANSYS Explicit Dynamics they are established through the principle of conservation of mass, momentum and energy. The finite element analysis itself is a study of continuum, therefore another two relationships describing the material behavior is required, namely the Equation of State (EOS) and a constitutive material model. RHT concrete model combines the strength model and failure model that form the constitutive material model in a single formulation [13], [14]:

$$F_{fail}\left(P, \sigma_{eq}, \theta, \varepsilon_p, \dot{\varepsilon_p}\right) = \sigma_{eq} - \left[f_c \times Y^*\left(\varepsilon_p, P^*, \dot{\varepsilon_p}\right) \times F_{CAP}\left(P^*\right) \times R_3\left(\theta\right)\right])$$

$$Y^*\left(\varepsilon_p, P^*, \dot{\varepsilon_p}\right) = f_c\left[\varepsilon_p, Y^*_{TXC}\left(P^*, F_{RATE}\left(\dot{\varepsilon_p}\right)\right)\right]$$

where
σ_{eq} = equivalent stress,
f_c = uniaxial compressive strength,
$Y*(\varepsilon_p, P^*, \dot{\varepsilon_p})$ = pre-peak yield surface on the compressive meridian,
P = pressure,
P^* = pressure normalized by the uniaxial compressive strength,
θ = Lode angle,
ε_p = plastic strain,
$\dot{\varepsilon_p}$ = plastic strain rate,
F_{CAP} = pressure dependent elastic cap function,
$R_3(\theta)$ = third invariant dependency,
$Y^*_{TXC}(P^*, F_{RATE}(\dot{\varepsilon_p}))$ =pressure and rate dependent peak surface on the compressive meridian and
$F_{RATE}(\dot{\varepsilon_p})$ = strain rate dependency.

The strain rate independent compressive meridian in RHT formulation is developed through the following equations:

$$Y^*_{TXC}(P^*) = A(P^* - P^*_s)^n$$

$$P^*_s = \frac{1}{3} - \left(\frac{1}{A}\right)^{\frac{1}{n}}$$

Where:
A and *n are the failure surface parameters that define the shape of the failure surface as a function of pressure. On the other hand, P_s* is the spall strength.*

Strain rate effects are incorporated into the equation through the increases in peak strength. Two different terms are used for compression and tension, defined as:

$$F_{RATE} = \begin{cases} \left(\frac{\dot{\varepsilon}}{\dot{\varepsilon_o}}\right)^{\delta} \\ \left(\frac{\dot{\varepsilon}}{\dot{\varepsilon_o}}\right)^{\alpha} \end{cases}$$

where
F_{RATE} = represents the dynamic increase factor (DIF) as the function of strain rate $\dot{\varepsilon}$,
α and δ = user defined parameters and
$\dot{\varepsilon_0}$ = reference strain rate (quasi-static).

The minimum value F_{RATE} is 1.0. This rate enhancement factor is applied to the peak strength surface using the equations:

$$Y^*_{TXC}\left(P^*, F_{RATE}(\dot{\varepsilon})\right) = A_{dyn}(P^* - P^*_{s,dyn})^n$$

$$A_{dyn=} AF^{1-n}_{RATE}$$

$$P^*_{s,dyn} = F_{RATE}\left(\frac{1}{3} - \frac{1^{\frac{1}{n}}}{A}\right)$$

Figure 5 shows a typical deviatoric section plane of a strength surface. In the case of concrete material, the deviatoric section changes from triangular shape at low pressure (brittle condition) to a circular shape at high pressure (ductile

condition). In RHT concrete model, the transition is represented through the third invariant dependent term $R3(\theta)$ and evaluated by the following equations:

$$R_3(\theta) = \frac{2(1-\psi^2)cos\theta+(2\psi-1)(4(1-\psi^2)cos^2\theta+5\psi^2-4\psi)^{\frac{1}{2}}}{4-(1-\psi^2)cos^2\theta+(1-2\psi)^2}$$

$$\psi = \psi_0 \times B_Q \times P^*$$

$$\cos(3\theta) = \frac{3(3)^{\frac{1}{2}}\times j_3}{(2)^{\frac{3}{2}}\times(j_2)^{\frac{1}{2}}}$$

where
ψ = ratio of a material tensile strength to compressive strength,
ψ_0 = tensile to compression meridian ratio at zero pressure,
B_Q = rate at which the fracture surface transits from a triangular to a circular form with increasing pressure and
J_2 & J_3 = second and third invariants of the deviatoric stress tensor

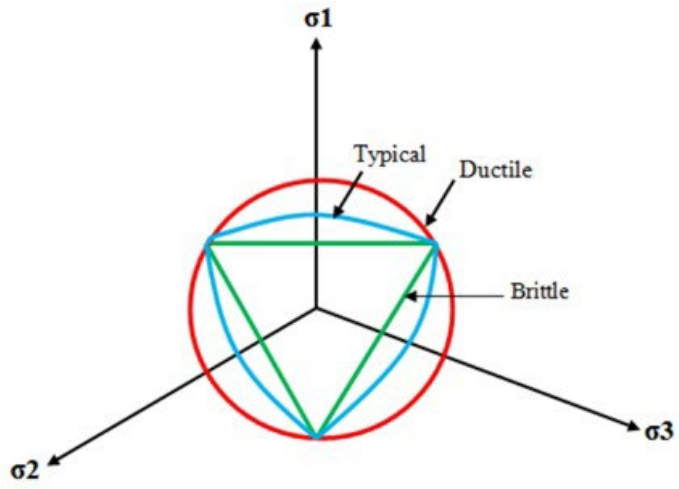

Figure 5- Deviatoric cross section of a strength surface

Figure 6 illustrates the concept of strain hardening based on a uniaxial compression curve. In order to allow for strain hardening behaviour, an elastic limit surface and a hardening slope is introduced. The elastic limit surface is scaled down from the peak surface by the normalized elastic strength parameters (user defined). The pre-peak yield surface is defined through the interpolation between the elastic and peak surfaces based on the ratio of elastic and plastic shear moduli using:

$$Y^* = \frac{\varepsilon_p}{\varepsilon_{p,pre}}(Y^*_{TXC} - Y^*_{el}$$

$$\varepsilon_{p,pre} = \frac{Y^*_{TXC}}{3G} \times \frac{G}{G-G_{pl}}$$

where
Y^*_{el} = initial elastic limit scaled down from peak surface,

ε_p = plastic strain, accumulated as soon as elastic surface is exceeded,
$\varepsilon_{p,pre}$ = pre-peak plastic strain,
G = shear modulus and
G_{pl} = plastic shear modulus.

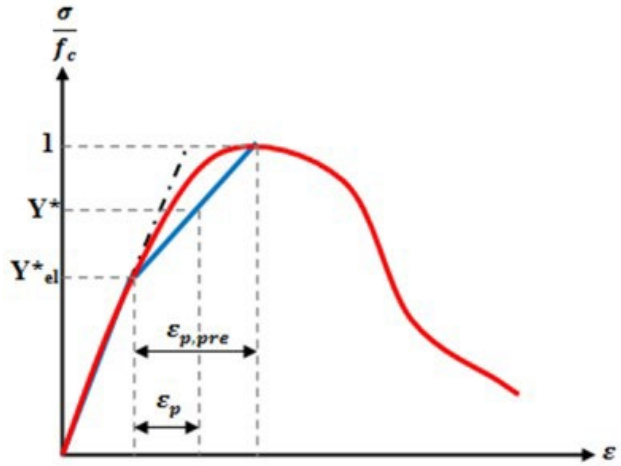

Figure 6- Concept of strain hardening in RHT concrete model

Damage is assumed to accumulate due to the shear induced cracking once the peak yield has been exceeded. A damage index D is used to determine the value of the current strength surface using the relationship:

$$D = \sum \frac{\Delta_{\varepsilon_p}}{\varepsilon_p^{fail}}$$

$$\varepsilon_p^{fail} = MAX(D1(P^* - htl^*)^{D2}, \varepsilon_{p,min}^{fail}$$

$$htl^* = -\frac{f_t}{f_c} \times \frac{f_s}{f_c} \times \psi_0 \left(\frac{\frac{f_t}{f_c}}{3\left(\psi_0 \frac{f_s}{f_c} - \frac{f_t}{f_c}\right)} \right)$$

where
D = damage index (ranging from zero to unity),
$D1$ & $D2$ = damage constants,
ε_p^{fail} = pressure dependent plastic strain to failure,
$\varepsilon_{p,min}^{fail}$ = minimum strain to failure (complete damage at low pressure),
htl^* = normalized hydrodynamic tensile limit,
f_t / f_c = normalized tensile strength and
f_s / f_c = normalized shear strength.

The strength of the completely crushed material in the present model is defined through the reduction in strength (strain softening) using equation:

$$Y_{res} = (B \times (P^*)^m)$$

Where:
Y_{res} = residual strength surface and
B & m = residual strength parameters.

On the other hand, the current shear modulus of the crushed material $G_{fractured}$ is defined through:

$$G_{fractured} = (1 - D)G + DG_{residual}$$

where
$G_{residual}$ = residual shear modulus at fracture (post-damage shear).

In the present work, the strength of CONC-35 was set to 40 MPa for the normal strength concrete material for which the density value was set to 2350 kg/m3. The shear modulus of concrete was calculated as 11,976 MPa which is 40 percent of the concrete's modulus of elasticity which is 29,940 MPa. Initial compaction pressure was considered as 16.7 MPa. On the other side, the strength of CONC-140 was set to 145 MPa for UHPC and tensile strength equal 22 MPa (f_t / f_c = 0.15).

The RHT concrete model parameters for both NRC & UHPC used in the present numerical analysis are summarized in Table 2.

Table 2 - Material model properties for RHT concrete model [10], [14]

Name	Units	NRC	UHPC
Density	t/mm^3	2.5 e-09	2.7 e-09
Poisson's ratio	None	0.20	0.20
Compressive strength	MPa	40	145
Tensile to comp. strength (f_t/f_c)	None	0.08	0.15
Shear strength to compressive (f_s/f_c)	None	0.18	0.18
Intact failure surface constant A	None	1.6	1.6
Intact failure surface exponent N	None	0.61	0.61
Tens./Comp. Meridian ratio Q2.0	None	0.6805	0.6805
Brittle to Ductile Transition BQ	None	0.0105	0.0105
Hardening Slope	None	2	2
Elastic Strength/ft	None	0.7	0.7
Elastic Strength/fc	None	0.53	0.53
Residual Strength constant B	None	1.6	1.6
Residual Strength constant M	None	0.61	0.61
Compressive strain rate exponent, á	None	0.029	8.79e -03
Tensile strain rate exponent, ä	None	0.034	0.012
Maximum fracture strength ratio SFMAX	None	1E+20	1E+20
Use cap on elastic surface	None	Yes	Yes
Damage Constant D1	None	0.04	0.04
Damage Constant D2	None	1	1
Minimum strain to failure	None	0.01	0.01
Residual shear modulus fraction	None	0.13	0.13
Shear Modulus	MPa	11,976	22,802
Porous Sound speed	mm/s	2897E03	3242E03
Initial Compaction Pressure Pe	MPa	18.37	93.30
Solid Compaction Pressure Ps	MPa	6000	6000
Compaction Exponent n	None	3	3

4.2.2 Constitutive model of reinforcement

Steel bars reinforcement were simulated by Steel 4340 model which is implement in Ansys Workbench library. The behavior of Steel 4340 is defined by Johnson-Cook strength and failure model. Johnson-Cook model was used to define strength of the material Steel 4340. This constitutive model defines the strength behavior of materials subjected to large strains, high strain rates and high temperatures [15]

$$Y = \left[A + B\varepsilon_p^n\right]\left[1 + c\ log\varepsilon_p^n\right][1 - T_H^m] \quad (1)$$

Where:
ε_p= effective plastic strain
ε_p*= normalized effective plastic strain rate
T_H = homologous temperature = $(T - T_{room})/ (T_{melt} - T_{room})$

The used parameters of Johnson - Cook damage model of steel reinforcement [15] is shown in Table 3.

Table 3- Johnson-Cook constitutive parameters for steel 4340 model [15]

Material	Density	õ	E	$\acute{o}_y$(A)	B	n	m	C	Tmelt	Troom
Steel 4340	7.8E-009 t/mm^3	0.3	200,000 MPa	360 MPa	1500 MPa	0.4	1.2	0.045	1800 K	293 K

Where:
A: Yield stress of the used steel bars is taken as 360MPa & Youngs modulus = 200,000MPa [10]
B, n, m and C are material constants

Constitutive Model of Explosive Material

TNT (Explosive). The TNT is defined using Jones-Wilkins-Lee (JWL) form of equation of state

$$P = A[1 - \omega/R_1V\ ]e^{-R1V} + B[1 - \omega/R_2V]e^{-R2V} + \ \omega E/V \quad (2)$$

Where A, B, R1, R2, are empirically derived constants varies with each explosive, V is the relative volume of expansion of explosive product and E is the detonation energy per initial unit volume [16]. The material property of TNT and variable for JWL equations listed in Table 4.

Table 4- Jones-Wilkins-Lee (JWL) constitutive parameters for TNT

Variable	Value
Density, kgm^3	1.225
A	373.77
B	374.71
R1	4.15
R2	0.9
ù	0.35
C-J Detonation velocity (m/ms)	6.93
C-J Energy/unit volume (MJ/m^3)	6000
C-J Pressure (Mpa)	21000

4.3 Boundary Conditions

Boundary conditions of the finite element models were simulated accurately like experiential ones. Both ends of the slab were fixed. As reported by Li et al. [10] that contact explosion which induces highly localized response and damage does not depend on the boundary condition.

4.4 Steel-Concrete Bond

The bond between steel reinforcement and concrete in the FE models were simulated as full bonded. Because the govern failure and damage modes is sudden local material damage and fragmentations which will occurs before bond slippage.

4.5 Finite Element Analysis

The finite analysis was carried out using ANSYS Workbench Explicit Dynamic Version 2021R2 [11]. This widely and famous used software is capable of solving problems including impact, explosions, collusions and material failure

using a Lagrange solver. Users can run the software as part of ANSYS workbench environment. For contact explosion test simulation, coupled finite element and smoothed particle hydrodynamics (SPH) method is adopted(FEM-SPH), coupled FEM-SPH algorithm is the most effective method to reproduce the damage progresses of the RC slab to contact explosion as investigated by Zhao et al. [12]. The SPH particles are used to simulate the high explosive and finite elements are used to simulate the reinforced concrete slab.

4.5.1 Mesh sensitivity

For studying the element mesh sizes whether it affects the analysis or not, the slabs have been modeled using three different mesh sizes of 10 mm, 20 mm, and 30 mm respectively. Table 5 shows the details of the mesh data for the current slab model. For each slab, refined element mesh sizes have been used to carry out the analysis and a comparison of experiential results with FE ones has been conducted to see the best size which gives more accurate results and damage shapes.

Table 5: Mesh size data for slab (NRC-2) model

	Mesh 1	**Mesh 2**	**Mesh 3**
Mesh Size	10 mm	20 mm	30 mm
Nodes	223093	34443	13144
Elements	197929	26725	9023

From the above trails, the slab specimens using the 20 mm mesh size can be used to show clearly the crack propagation of the slab system with more refined eroded particles than the coarser mesh(30mm). 20 mm mesh size will be used for all FE models; it gave more accurate results with reasonable computational time.

4.5.2 Analysis types

Dynamic explicit analysis is performed for all cases. Solutions are computed up to 500 μs, where no further permanent deformation is observed for all load values.

5 RESULTS AND DISCUSSIONS

5.1 Validation of the Proposed FE Models

One critical aspect of numerical simulations is validation with experimental results or physical phenomenon to ensure the accuracy of selected material models, boundary conditions, and contact algorithms adopted in the established FE model.

5.2 Normal Strength Concrete (NRC) Slab

Based on the experimental work of Li et al. [10], the normal strength concrete slab NRC-2 was subjected to 1 kg TNT contact explosion placing also at the center of slab surface. As can be noticed from Figures 7, and 8 severe blast load induced perforation or punching failure in the slab. It is also noted that significant concrete cracking occurred along the two free (unsupported) edges near the slab boundary. As no clear slab deformation was observed, these damages were believed also caused owing to the following reasons:

1- Stress wave propagation

2- Reflection

Stress wave of contact explosion caused cracks along the two unsupported edges because of the short propagation distance between the contact TNT explosive material and the free boundary edges, which produced high tensile stresses which is extremely bigger than the concrete tensile strength due to wave reflection and thus cracking of concrete.

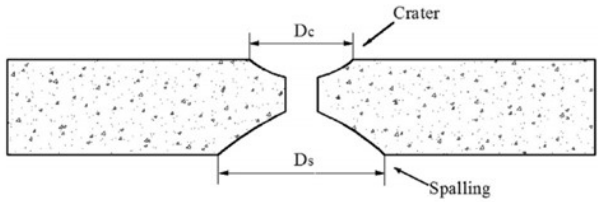

Figure 7-Measurement of the damaged areas

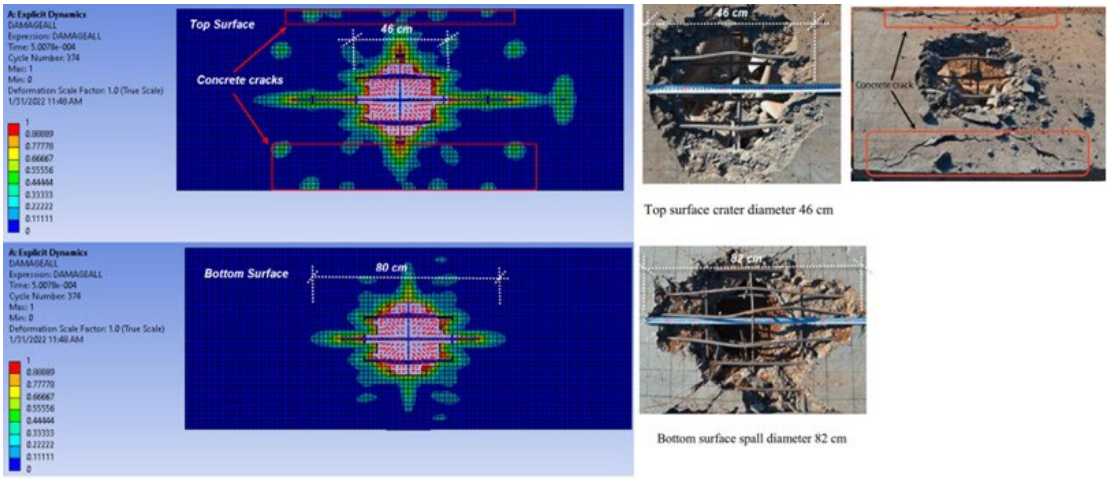

Figure 8 – Comparison between experimental damage & FE damage of NRC-2 Slab

5.3 Damage Pattern of RC Slab under Contact Explosion

Damage behavior of RC slabs under contact explosion refers to the dimensions of the crater and spalling of the NRC-2 slab. The level of damaged is estimated by the crater diameter (D_C) and spalling diameter (D_S). These values measured in both experiential work conducted by Li et al. [10] and the current FE models as illustrated in Table 6.

Table 6 - The diameters of the crater and spalling from the numerical simulations and experimental test

Slab	Damage Failure	Experimental Test [10]	FEM-SPH	EXP/FEM
NRC-2 Slab	Concrete Crater Top Surface	46	46	1
	Concrete Spalling Bottom Surface	82	80	1.025
UHPC-4 Slab	Concrete Crater Top Surface	23	24	0.96
	Concrete Spalling Bottom Surface	45	48	0.94
UHPC-7Slab	Concrete Crater Top Surface	25	26	0.96
	Concrete Spalling Bottom Surface	48	50	0.96

The damage diameters of the crater and spalling are found in Figures 7 and 8. The contour value between 0 and 1 indicates the concrete element damage [0: undamaged material & 1: fully damaged material]. As shown in Figure 8, the elements with damage values between 0.9 to 1.0 are not shown. The purpose of such processing is to better and clearly show the damage status of the RC slab. This is because when the damage values of the damage zone are between 0.9 and 1.0, the concrete material has been severely damaged. Lots of macroscopic cracks will appear in the damaged region of the RC slab, and the SPH particles

have been flying. Under contact blast conditions, the blast pressure directly impacts the top surface and causes a crater failure which is approximately circular and localized at the middle of the slab.

The crater diameters for the FEM-SPH is about 46 cm. When the blast pressure impacts the top surface of the RC slab, it induces a punching failure. Meanwhile, the interaction between the incident stress and reflective stress causes a spalling failure on the bottom surface of the RC slab. The spalling failure diameters for the FEM-SPH is about 80 cm. Table 6 shows the diameters of the crater and spalling from the numerical simulations and experimental test, it appears that a good matching between both results was achieved.

It is noted in both test slabs and numerical results, that the dynamic response of the RC slab is highly localized in the contact explosion at the middle of the slab. The global flexural behavior of the slab has not been observed in the RC slab and is expected to be very small. Due to the lack of the deformation and strain data of the test slab, only the failure mode and failure dimension (D_C & D_S) are compared between the test slabs and numerical results. As can be clearly seen, the damage profiles from the numerical models all match reasonably with the experimental results of Li et al. [10] in terms of the diameters of the crater and spalling. Overall, it may be concluded that the FE models created by FEM-SPH method can effectively predict the damage processes of the RC slabs subjected to contact explosion.

Based on FEM-SPH method, the top crater, punching and bottom spalling of the RC slab are all well reproduced, and the deformation and failure modes of the reinforcement steel bars are also well predicted.

Figure 6 shows the comparison between experimental damage profile of the NRC-2 slab exposed to contact explosion obtained from the experimental test conducted by Li et al. [10] & FEM-SPH model, good matching is observed. Figure 9 shows comparison between experimental & FE results of the recorded strain time histories on reinforcement bars detected by strain gauge at the center (Point 1) of NRC-2 Slab. Very good accuracy was achieved in the current FE methodology, Exp./ FE results of long. steel bars at center =1.04.

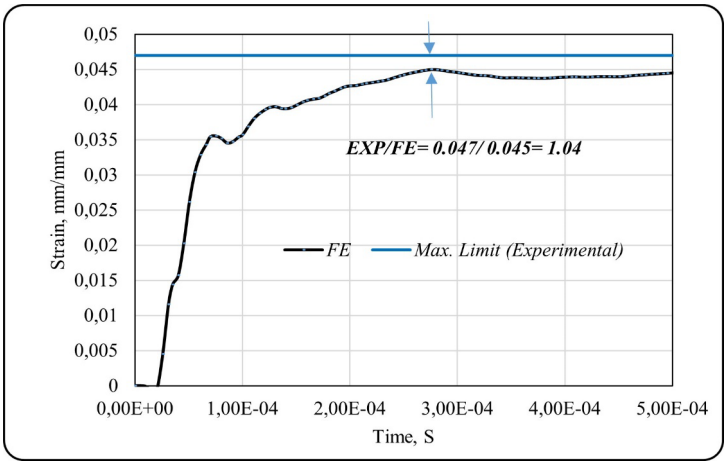

Figure 9 -Comparison between experimental & FE results of steel strain detected by strain gauge at the center (Point 1) of NRC-2 Slab

5.4 Ultra-High Performance Concrete Slab

The proposed finite element model showed the UHPC material's ability to effectively resist contact explosion. UHPC-4 slab was tested experimentally and modeled numerically with a 1 kg TNT detonated at its central surface. The damage behavior of UHPC-4 slab is similar as NRC-2, which is localized punching or perforation failure (crater and spalling). A very good matching of damage mode was attained between tested UHPC-4 slab and FE simulated one as shown in Figure 10. It was noted that UHPC-4 slab has better blast resistance capacity compared with NRC-2 slab under the same blast load condition. The top surface crater diameter and the bottom surface spall diameter were reduced from 46 cm and 82 cm to 23 cm and 45 cm (50% and 45%,) respectively. Accurate Predicted values of D_C & D_S are noticed in Table 6. Moreover, no side concrete cracking as in NRC-2 was observed, and no reinforcement fracture was observed either. These comparisons clearly demonstrate the better blast loading resistance capacity of UHPC than normal concrete. To show more accuracy of the model, Figure 11 shows comparison between experimental & FE results of the recorded strain time histories on reinforcement bars detected by fixed strain gauge in long. steel bars at center of slab (Point 1) of UHPC-4 Slab. Very good accuracy was achieved in the current FE methodology, Exp./ FE results =0.95

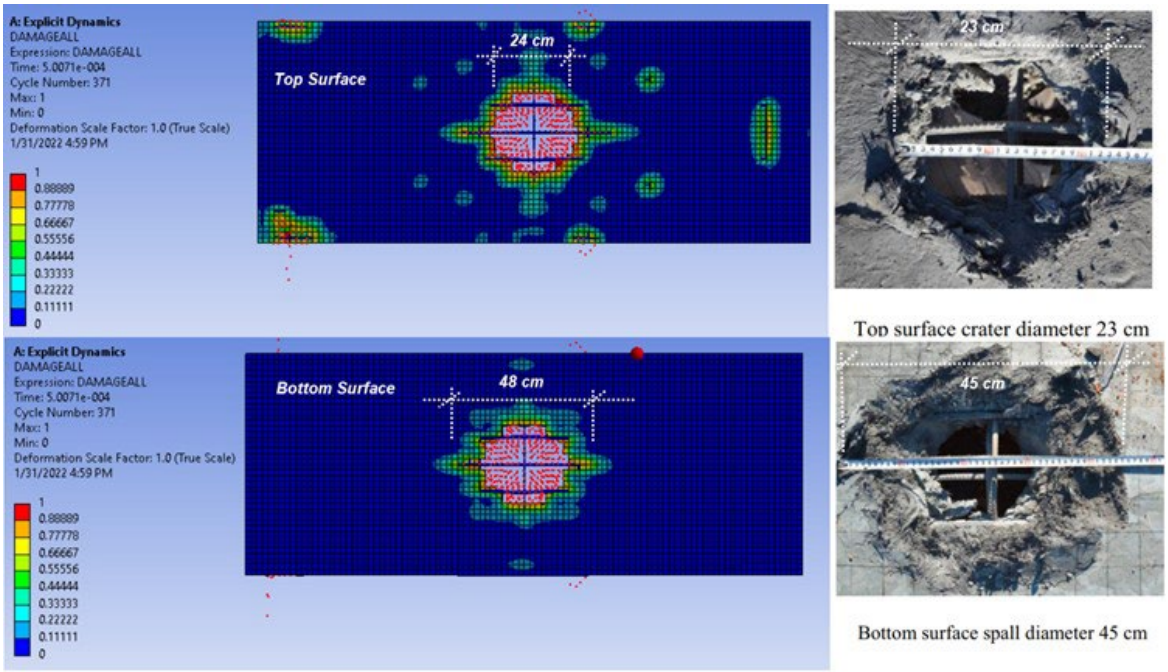

Figure 10– Comparison between experimental damage & FE damage of UHPC-4 Slab

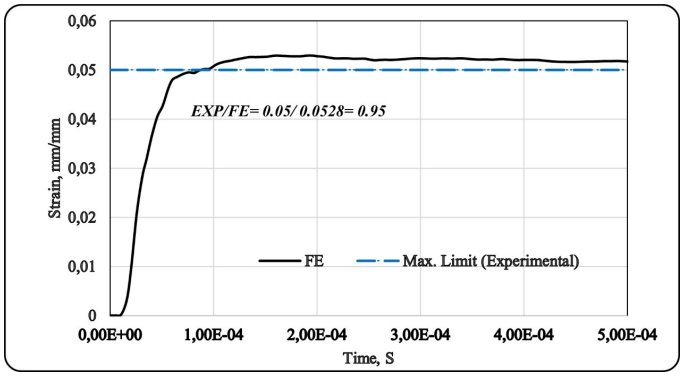

Figure 11 -Comparison between experimental & FE results of steel strain detected by strain gauge at the center (Point 1) of UHPC-4 Slab

To investigate the reinforcement mesh confinement effect on spalling damage, UHPC-7 slab was made the same as UHPC-4 but with less number of the longitudinal reinforcements in both the compressive and tensile face, i.e., the number of longitudinal reinforcement bars is reduced to 5 from 9. The slab was also tested experientially under 1.0 kg contact explosion and modeled numerically with the same FE approach used in the previous models. Comparison was made between UHPC-7 and UHPC-4 to investigate the influence of reinforcement mesh confinement effect on concrete crushing and spalling damages. A severe localized punching failure was observed. Comparing with UHPC-4, the top surface crater diameter and bottom surface spall diameter increased from 23 cm and 45 cm to 25 cm and 48 cm, respectively. As seen in Figure 12 and Table 6 that the used FE model accurately represent the real behavior and damage failure of tested UHPC-7 slab. Besides, the proposed FE model also shows good matching of deformation & buckling of longitudinal reinforcement at mid span with tested one as shown in Figure 13, which was not observed in UHPC-4. Generally speaking, the reinforcement mesh contributed to the resistance against the contact blast loads experimentally and numerically. Regarding measuring of steel strain with time, the strain detected by fixed strain gauge in long. steel bars at center of the slab (Point 1) of UHPC-7 Slab, current FE model matched well with tested one with ratio = 1.02 as shown in Figure 14.

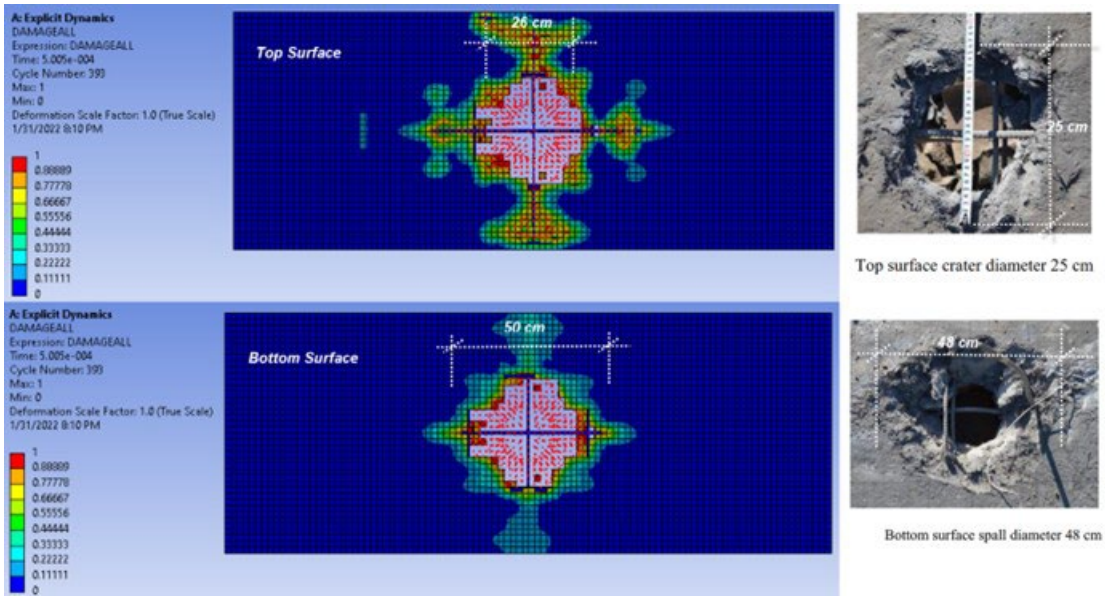

Figure 12 – Comparison between experimental damage & FE damage of UHPC-7 Slab

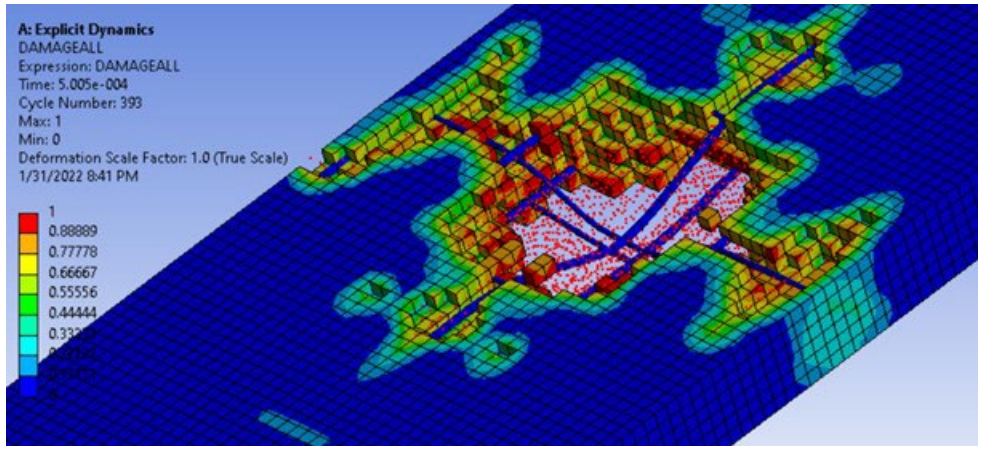

Figure 13 Deformation and steel buckling at mid of UHPC-7 Slab

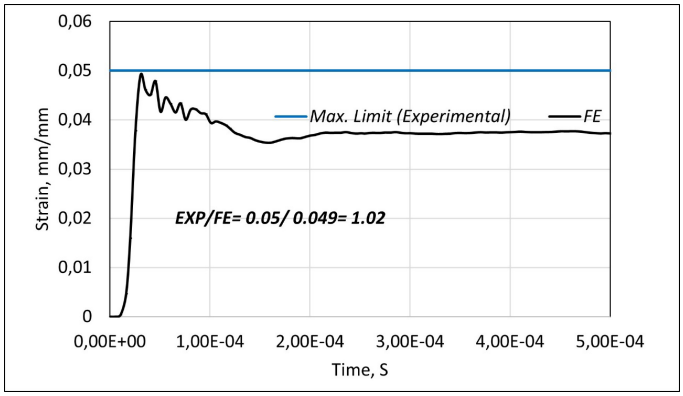

Figure 14-Comparison between experimental & FE results of steel strain detected by strain gauge at the center (Point 1) of UHPC-7 Slab

6 RETROFITTING PROPOSAL

6.1 Retrofitting of Normal Strength Concrete Slab by Bonded Steel Skin Layer

The above results and discussion indicate that the UHPC slab can resist the contact explosion with some permanent deformation and fragmentations better than NRC slab. To enhance the blast-resistance of both slabs, parametric studies are carried out to examine the retrofitting effect by bonded steel skin plates for top and bottom face of slabs upon the structural response under the contact blast scenario.

Two NRC slabs with steel skin thicknesses of 1 and 2 mm are compared in this section. The steel skin yield strength and the failure (erosion) strain of steel sheet were taken equal 330 MPa and 0.045 respectively as recommended in many papers [17]–[19].

The failure or damage occurs in slabs were monitoring by DAMAGEALL contour in Ansys Workbench Environment, which indicates to material damage: 0– intact material & 1- fully fractured. It is found that the NRC-2 slab retrofitted with 1 mm steel skin in both sides and exposed to 1 Kg TNT contact explosion experiences no perforation or punching failure and less central damage, compared to control one(experimental results of NRC-2 without retrofitting which damaged with perforation failure as shown in Figures 15 and 8).

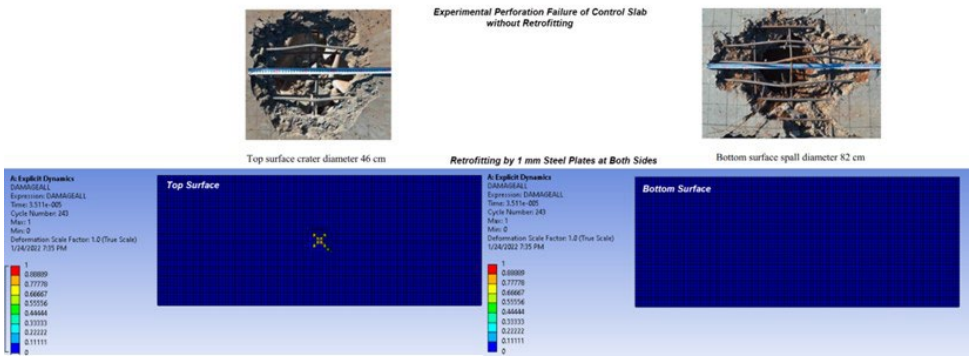

Figure 15 – Comparison between mode of failure of experimental non-retrofitted NRC-2 Slab and retrofitted NRC-2 by 1 mm steel skin plates at top & bottom surfaces

The increased thickness enhances the moment of inertia of steel skin. It can be concluded that increasing the skin thickness results in a significant improvement on the blast resistant performance. When the skin thickness increases from 1mm to 2 mm, the NRC-2 panel can attain the best performance against contact explosion. Retrofitting by 2 mm steel plate at both sides, leads to no damage, no punching failure, and no cracks were observed (Figure 16). Only central small deformation has been observed on the steel plate at top surface which adjacent to contact explosion.

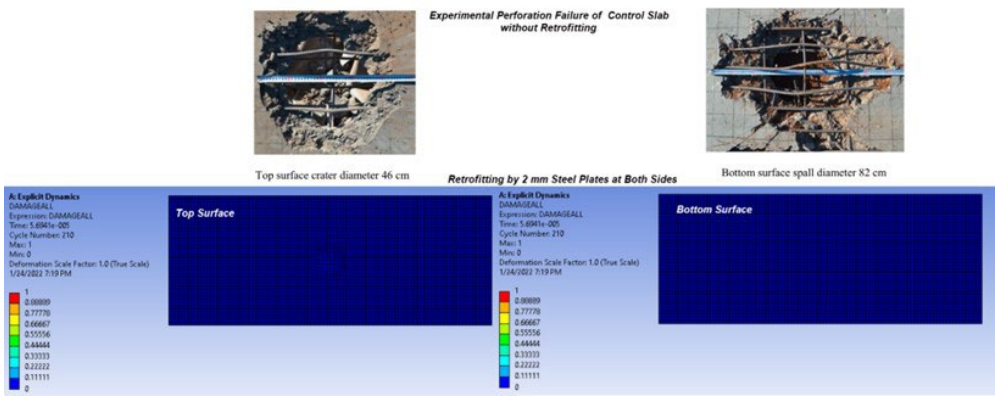

Figure 16– Comparison between mode of failure of experimental non-retrofitted NRC-2 Slab and retrofitted NRC-2 by 2 mm steel skin plates at top & bottom surfaces

6.2 Retrofitting of Ultra-High Performance Concrete Slab by Bonded Steel Skin Layer

Composite action generated from UHPC & 1mm bonded steel plates at both faces of the UHPC-4 slab has a superior resistance to contact blast. As clearly shown in Figure 17, a negligible damage in a few points at the top surface, and completely no damage occurs at bottom surface. Adequate protection is obviously shown compared with non-retrofitted one. By bonded steel plate retrofitting technique & UHPC material, no fragmentation is happened.

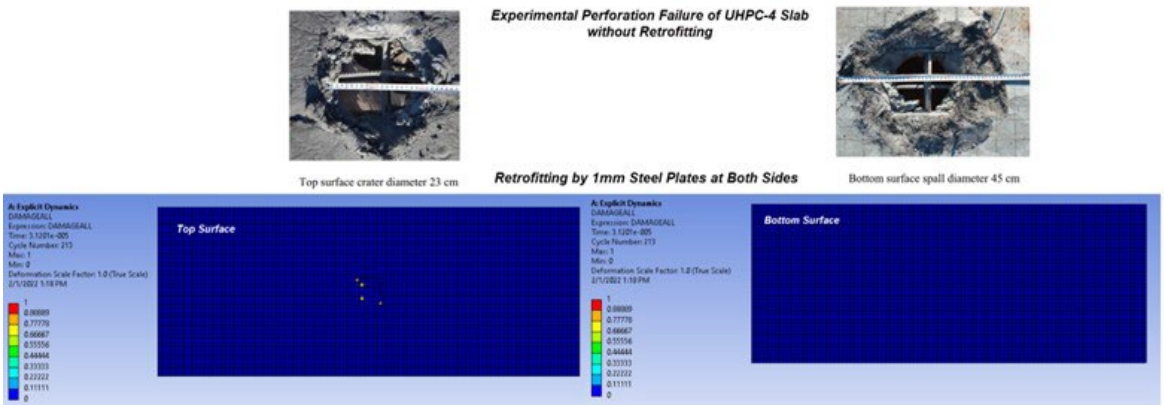

Figure 17 – Comparison between mode of failure of experimental non-retrofitted UHPC-4 Slab and retrofitted one by 1 mm steel skin plates at top & bottom surfaces

By analogy with the above, the use of 2mm bonded steel plate retrofitting will give more protection but, with more cost. For practical and economical use, 1 mm is enough to protect UHPC slab under 1 kg TNT contact explosion and adequate to prevent any fragmentation. To prove the previous phenomenon, Figure 16 shows bare concrete surfaces without covered plates. Regarding the upper surface of the concrete adjacent to the bottom of the covered plate, no punching damage is observed, just only small localized damage at slab center, which is negligible compared to UHPC-4 without retrofitting. The Figure 18 show also that 1 mm is very enough to completely protect the bottom surface without any damage, or not even any cracks.

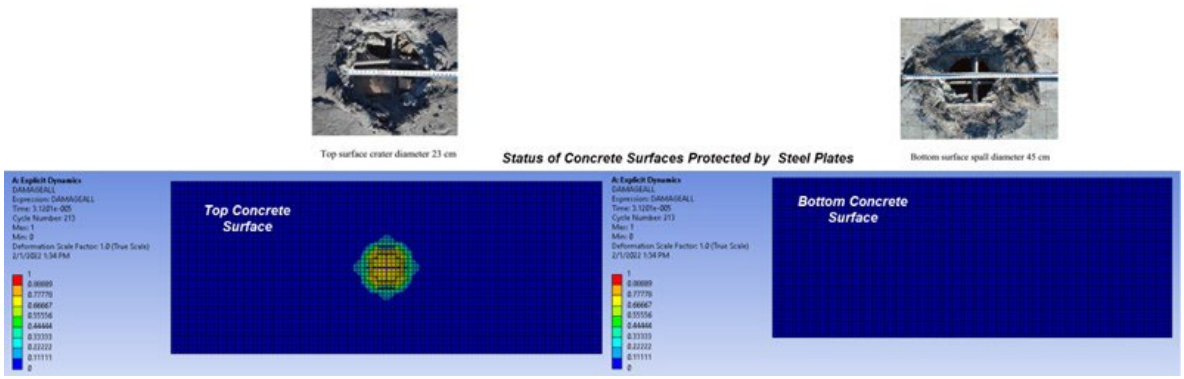

Figure 18-Status of top & bottom concrete surfaces of UHPC-4 slab protected by 1 mm steel plates at both surfaces.

7 CONCLUSIONS

The following are the main drawn concluding remarks:

1. In both test slabs and numerical results, the dynamic response of the both NRC & UHPC slabs is highly localized punching or perforation failure (crater and spalling) in the contact explosion at the middle of the slab.
2. The damage profiles from the numerical models all match reasonably with the experimental results of Li et al. [10] in terms of the diameters of the crater and spalling and steel strain. Overall, it may be concluded that the FE models created by FEM-SPH method can effectively predict the damage processes of the NRC and UHPC slabs subjected

to contact explosion. The suggested finite element model is valid to solve the reinforced concrete slab under contact-explosion problems. The top crater, punching and bottom spalling of the RC slab are all well reproduced, and the deformation and failure modes of the reinforcement steel bars are also well predicted.

3. ANSYS Workbench Explicit Dynamics and the RHT Concrete Damage model introduced powerful and reliable results to simulate the overall performance of NRC & UHPC slabs exposed to contact explosion.
4. UHPC slab has better blast resistance capacity compared with NRC slab under the same blast load condition. The top surface crater diameter and the bottom surface spall diameter were reduced by 50% and 45%, respectively. Moreover, no side concrete cracking like in NRC was observed, and no reinforcement fracture was observed either.
5. The influence of reinforcement mesh confinement effect upon concrete crushing and spalling damages is examined. With reducing the amount of reinforcement mesh confinement in compressive and tensile faces of the UHPC slab, a severe localized punching failure and buckling of longitudinal reinforcement at mid span were observed numerically and verified experimentally.
6. Steel skin plate retrofitting results in a significant improvement on the blast resistant performance. When the skin thickness increases from 1mm to 2 mm, the NRC panel can attain the best performance against contact explosion. Retrofitting of normal strength concrete slab by bonded 2mm steel skin plates of both sides significantly improved the blast resistance by preventing completely fragmentations and securing stability and proves to be an effective solution to eliminate contact- blast damage.
7. Composite action generated from UHPC & 1mm bonded steel plates at both faces of the UHPC slab has a superior resistance to contact explosion, it is very enough to completely protect against contact explosion with 1kg TNT, It has a superior resistance to contact blast, no perforation failure, and no cracks were observed.

ACKNOWLEDGEMENTS

The author wishes to thank the Ansys Co., for giving him Ansys Academic Version.

REFERENCES

[1] J. Li and H. Hao, "Numerical study of concrete spall damage to blast loads," *Int. J. Impact Eng.*, vol. 68, pp. 41–55, Jun 2014, http://dx.doi.org/10.1016/j.ijimpeng.2014.02.001.

[2] N. Gebbeken and M. Ruppert, "A new material model for concrete in high-dynamic hydro code simulations," *Arch. Appl. Mech.*, vol. 70, no. 7, pp. 463–478, 2000, http://dx.doi.org/10.1007/s004190000079.

[3] M. Mines, A. Thach, S. Mallonee, L. Hildebrand, and S. Shariat, "Ocular injuries sustained by survivors of the Oklahoma City bombing," *Ophthalmology*, vol. 107, no. 5, pp. 837–843, May 2000, PMid:10811071.

[4] S. Mallonee, S. Shariat, G. Stennies, R. Waxweiler, D. Hogan, and F. Jordan, "Physical injuriesand fatalities resulting from the Oklahoma City bombing," *JAMA*, vol. 276, no. 5, pp. 382–387, Aug 1996, http://dx.doi.org/10.1001/jama.1996.03540050042021.

[5] B. Brismar and L. Bergenwald, "The terrorist bomb explosion in Bologna, Italy, 1980: an analysis of the effects and injuries sustained," *J. Trauma Inj. Infect. Crit. Care*, vol. 22, no. 3, pp. 216–220, Mar 1982, http://dx.doi.org/10.1097/00005373-198203000-00007. PMid:7069805.

[6] M. Morishita, H. Tanaka, T. Ando, and H. Hagiya, "Effects of concrete strength and reinforcing clear distance on the damage of reinforced concrete slabs subjected to contact detonations," *Concr. Res. Technol.*, vol. 15, no. 2, pp. 89–98, Jan 2004, http://dx.doi.org/10.3151/crt1990.15.2_89.

[7] H. Tanaka and M. Tuji, "Effects of reinforcing on damage of reinforced concrete slabs subjected to explosive loading," *Concr. Res. Technol.*, vol. 14, no. 1, pp. 1–11, 2003, http://dx.doi.org/10.3151/crt1990.14.1_1.

[8] J. Nam, H. Kim, and G. Kim, "Experimental investigation on the blast resistance of fiber reinforced cementitious composite panels subjected to contact explosions," *Int. J. Concr. Struct. Mater.*, vol. 11, no. 1, pp. 29–43, Feb 2017, http://dx.doi.org/10.1007/s40069-016-0179-y.

[9] F. Toutlemonde and J. Resplendino, *Designing and Building with UHPFRC: State of the Art & Development.* Hoboken: John Wiley & Sons.

[10] J. Li, Ch. Wu, H. Hao, Zh. Wang, and Y. Su, "Experimental investigation of ultra-high performance concrete slabs under contact explosions," *Int. J. Impact Eng.*, vol. 93, pp. 62–75, Jul 2016, http://dx.doi.org/10.1016/j.ijimpeng.2016.02.007.

[11] ANSYS, *Finite Element Analysis Program, 2021R2 Release*. USA: SAS IP Inc., 2021.

[12] X. Zhao, G. Wang, W. Lu, P. Yan, M. Chen, and Ch. Zhou, "Damage features of RC slabs subjected to air & underwater contact explosions," *Ocean Eng.*, vol. 147, pp. 531–545, Jan 2018, http://dx.doi.org/10.1016/j.oceaneng.2017.11.007.

[13] W. Riedel, K. Thoma, S. Hiermaier, and E. Schmolinske, “Penetration of reinforced concrete by beta-b-500, numerical analysis using a new macroscopic concrete model for hydrocodes,” in *Proc. 9th Int. Symp. Interact. Eff. Mun. Struct.*, Strausberg, Berlin, 1999, pp. 315-322. CD-ROM.

[14] T. Borrvall and W. Riedel, “The RHT concrete model in LSdyna,” in *Proc. 8th Eur. LS-DYNA Users Conf.*, Strasbourg, France, 2011.

[15] G. R. Johnson and W. H. Cook, “A constitutive model and data for metals subjected to large strains, high strain rates and high temperatures,” in *Proc 7th Int. Symp. Ballis.*, The Netherlands, 1983.

[16] A. Hameed, “Numerical analysis of vehicle bottom structures subjected to anti-tank mine explosions,” Ph.D. dissertation, Canfield Univ., 2008.

[17] Y. Cui, M. Song, Z. Qu, S. Sun, and J. Zhao, "Research on damage assessment of concrete-filled steel tubular column subjected to near-field blast loading," *Shock Vib. J.*, vol. 2020, pp. 8883711, 2020, http://dx.doi.org/10.1155/2020/8883711.

[18] D. Thai, T. Pham, and D. Nguyen, "Damage assessment of reinforced concrete columns retrofitted by steel jacket under blast loading," *Struct. Des. Tall Spec. Build.*, vol. 29, no. 1, e1676, 2020, http://dx.doi.org/10.1002/tal.1676.

[19] H. Draganić, G. Gazić, and D. Varevac, "Experimental investigation of design and retrofit methods for blast load mitigation: a state-of-the-art review," *Eng. Struct.*, vol. 190, pp. 189–209, Jul 2019, http://dx.doi.org/10.1016/j.engstruct.2019.03.088.

Author contributions: IMM: conceptualization, formal analysis, writing.

Editors: Bruno Briseghella, Guilherme Aris Parsekian.